

---

This is an electronic reprint of the original article.  
This reprint may differ from the original in pagination and typographic detail.

Emelianov, Aleksei V.; Nekrasov, Nikita P.; Moskotin, Maksim V.; Fedorov, Georgy E.; Otero, Nerea; Romero, Pablo M.; Nevolin, Vladimir K.; Afinogenov, Boris I.; Nasibulin, Albert G.; Bobrinetskiy, Ivan I.

## Individual SWCNT Transistor with Photosensitive Planar Junction Induced by Two-Photon Oxidation

*Published in:*  
Advanced Electronic Materials

*DOI:*  
[10.1002/aelm.202000872](https://doi.org/10.1002/aelm.202000872)

Published: 01/03/2021

*Document Version*  
Peer reviewed version

*Please cite the original version:*  
Emelianov, A. V., Nekrasov, N. P., Moskotin, M. V., Fedorov, G. E., Otero, N., Romero, P. M., Nevolin, V. K., Afinogenov, B. I., Nasibulin, A. G., & Bobrinetskiy, I. I. (2021). Individual SWCNT Transistor with Photosensitive Planar Junction Induced by Two-Photon Oxidation. *Advanced Electronic Materials*, 7(3), [2000872].  
<https://doi.org/10.1002/aelm.202000872>

---

This material is protected by copyright and other intellectual property rights, and duplication or sale of all or part of any of the repository collections is not permitted, except that material may be duplicated by you for your research use or educational purposes in electronic or print form. You must obtain permission for any other use. Electronic or print copies may not be offered, whether for sale or otherwise to anyone who is not an authorised user.

**Individual SWCNT Transistor with Photosensitive Planar Junction Induced by Two-Photon Oxidation**

*Aleksei V. Emelianov,\* Nikita P. Nekrasov, Maksim V. Moskotin, Georgy E. Fedorov, Nerea Otero, Pablo M. Romero, Vladimir K. Nevolin, Boris I. Afinogenov, Albert G. Nasibulin, and Ivan I. Bobrinetskiy*

Dr. A.V. Emelianov, N.P. Nekrasov, M. V. Moskotin, Prof. V.K. Nevolin, Dr. B.I. Afinogenov, Dr. I.I. Bobrinetskiy  
National Research University of Electronic Technology, 1 Shokin square, Moscow, Zelenograd 124498, Russia  
E-mail: emmsowton@gmail.com

Dr. A.V. Emelianov  
P.N. Lebedev Physical Institute of the Russian Academy of Sciences, 53 Leninsky prospect, Moscow 119991, Russia

M.V. Moskotin  
Moscow State University of Education, 1/1 Malaya Pirogovskaya Street, Moscow 119991, Russia

M.V. Moskotin, Dr. G.E. Fedorov  
Moscow Institute of Physics and Technology, 9 Institutskiy alley, 141701, Dolgoprudny, Russia

N. Otero, P.M. Romero  
Laser Applications Centre, AIMEN, 27A Calle Relva, Porriño 36410, Spain

Dr. B.I. Afinogenov  
Moscow State University, Faculty of Physics, 1–2 Leninskiye Gory, GSP-1, Moscow 119991, Russia

Prof. A.G. Nasibulin  
Skolkovo Institute of Science and Technology, 30/1 Bolshoy Boulevard, 121205, Moscow, Russia

Prof. A.G. Nasibulin  
Aalto University, Department of Applied Physics, 1B Otakaari, Aalto 00076, Finland

Dr. I.I. Bobrinetskiy  
BioSense Institute, University of Novi Sad, 1 Dr Zorana Djindjica, Novi Sad 21000, Serbia

Keywords: carbon nanotube, femtosecond laser, two-photon absorption, photodetector, photovoltaic

The fabrication of planar junctions in carbon nanomaterials is a promising way to increase the optical sensitivity of optoelectronic nanometer-scale devices in photonic connections, sensors, and photovoltaics. Utilized a unique lithography approach based on direct femtosecond laser

processing, a fast and easy technique for modification of single-walled carbon nanotubes (SWCNT) optoelectronic properties through localized two-photon oxidation is developed. It results in a novel approach of quasi-metallic to semiconducting nanotubes conversion so that metal/semiconductor planar junction is formed via local laser patterning. The fabricated planar junction in the field-effect transistors based on individual SWCNT drastically increases the photoresponse of such devices. The broadband photoresponsivity of the two-photon oxidized structures reaches the value of  $2 \cdot 10^7 \text{ A W}^{-1}$  per single SWCNT at 1 V bias voltage. The SWCNT-based transistors with induced metal/semiconductor planar junction can be applied to detect extremely small light intensities with high spatial resolution in photovoltaics, integrated circuits, and telecommunication applications.

## 1. Introduction

The density of integrated circuit elements increases rapidly according to Moore's law that approaches its limit with an element size reaching a nanometer-scale.<sup>[1]</sup> To overcome the limits of integration and overall performance of integrated circuits, novel approaches are suggested based on integrated optical communication on a chip.<sup>[2]</sup> The carbon nanotube (CNT)-based devices are very promising for an application in photonic integrated circuits owing to their small size and efficient light conversion.<sup>[3]</sup> Pristine nanotubes are up-and-coming candidates for IR light sensing,<sup>[4,5]</sup> while for broadband application, the tuning of CNT properties is necessary.<sup>[6]</sup> The photosensitivity of a CNT-based device may be achieved via different mechanisms, including photoconductive, photovoltaic, photogating, bolometric, and photothermoelectric effects.<sup>[7]</sup> Fabrication of a *p-n* junction in a CNT is one of the most efficient ways to get high photovoltaic responsivity and optical superresolution at the nanoscale spatial range.<sup>[8]</sup> The traditional way of a *p-n* junction formation is based on the multiple gating in CNT-based field-effect transistors (FET).<sup>[9-11]</sup> The maximum quantum yield of thus made *p-n* junction using a suspended nanotube was as high as 30 % for the

responsivity of about  $200 \text{ nA W}^{-1}$ .<sup>[12]</sup> Despite the evident advantages of formed *p-n* junctions for optoelectronics, the technological challenges related to their mass production are far from being resolved.

Another lithographic process is based on different doping from organic molecules deposited onto CNT and the formation of a *p-i-n* junction.<sup>[13]</sup> This technique provides a formation of a planar junction by changing the main charge carrier densities. Several methods for modifying the local optical properties in CNT are based on thermoelectrical contact formation by physical<sup>[14]</sup> or chemical modification.<sup>[15]</sup> Thus, chemical modification methods based on plasma treatment allow for the fabrication of a *p-n* junction in the nanotubes with defined properties depending on the irradiation dose.<sup>[16]</sup> Theoretical calculations predict that the increase of defects in zigzag nanotubes could convert them from metallic to semiconducting.<sup>[17]</sup> Additionally, experimentally controlled defect engineering demonstrates the local tunneling barrier generation in the area of single defects.<sup>[18,19]</sup> This barrier can very efficiently localize excitons that can be used in different photonic devices. Nevertheless, all these methods demand a complex device fabrication process that lacks further integration of a CNT-based photodetector in photonic schemes. The maskless direct writing methods of integrated photonic structures are highly desired.

The direct light-induced conversion of carbon nanotubes from metallic to semiconducting type is a promising but still challenging approach.<sup>[20]</sup> The light-induced defect generation in carbon lattice by oxygen chemical adsorption either in the form of epoxy or ether groups<sup>[17,21]</sup> is a high-potential method for local tuning of carbon nanomaterials properties. Moreover, several approaches for a nanotube local conversion by oxygen species grafting were suggested based on electrochemical doping<sup>[22]</sup> and plasmon-induced selective oxidation<sup>[23]</sup> that poses the local presence of nanoparticles near the nanotube. Recently, the direct laser writing methods of two-photon oxidation (TPO) of graphene and carbon nanotubes were demonstrated.<sup>[15,24]</sup> Interestingly, the effect of TPO is rather similar to less controllable

oxygen-induced radicals doping in the first stage of ozone treatment, when the destruction of the carbon atomic lattice has not yet begun.<sup>[25,26]</sup> TPO of the lattice by laser pulses with energies below the ablation threshold provides a novel tool for maskless patterning of the physical and chemical properties of CNT and graphene.<sup>[15,27,28]</sup> While the carbon surface is irradiated by ultrafast laser pulses (femto- or picosecond) at certain energies, both the grafting of oxygen-containing groups<sup>[29]</sup> and reconstruction of the hexagonal lattice<sup>[30,31]</sup> can be performed. This opens a new path of energy profile engineering in carbon nanostructures and other 1D and 2D materials. The local nature of irradiation allows the reconstruction of nanomaterials following a predefined pattern.

In this work, we describe an effective route to fabricate an ultrasensitive planar junction in individual single-walled CNT (SWCNT). The femtosecond laser (fs-laser) was used to process carbon nanotube transistors under standard conditions, and we demonstrate the converting of quasi-metallic (qm) to semiconducting (sc) nanotubes by local tuning of the morphology and structure, as well as alteration of electrical and optical properties of a part of the SWCNT channel. Moreover, the processed structures demonstrate a non-linear behavior of output electrical characteristics and the formation of an energy barrier near one of the contacts. We study the photocurrent generation upon continuous wave light-emitting diodes (LED) and fs-laser illumination in SWCNT FETs with a planar junction. We show a high photoresponsivity of more than  $50 \text{ mA W}^{-1}$  (or  $2 \cdot 10^7 \text{ A W}^{-1}$  per single SWCNT) for blue and UV light at ultralow intensities. Based on the experimental data, we found out that the observed ultrahigh photosensitivity is a result of an interplay between the photovoltaic and photogating effects.

## **2. Results and Discussion**

### **2.1. Two-Photon Oxidation of Individual SWCNT**

**Figure 1** illustrates the modification of the transistor characteristics of a typical SWCNT FET (the fabrication route for FET is shown in Figure S1, Supporting Information) as it undergoes the fs-laser processing (the scheme of the experiment is depicted in Figure S2, Supporting Information). A  $\sim 1 \mu\text{m}$  wide part of a nanotube was irradiated by the single passage of the fs-laser beam under standard conditions (20 °C, 1 atm, and 30 % humidity) (see Figure 1a). The dose of illumination was varied by adjusting the pulse energy and scanning speed of the laser beam (the number of pulses per  $\mu\text{m}^2$ ). The parameters of fifteen fs-laser processed and two pristine SWCNT FETs are summarized in Table S1, Supporting Information. Source and drain electrodes of the devices were connected to a digital multimeter for *in situ* resistivity measurements during laser illumination. We found that the SWCNT FET resistivity drastically changes upon irradiation of the channel with the laser beam at specific pulse energies (Figure S3, Supporting Information). This change is caused by TPO of the carbon surface and is irreversible.<sup>[30,32]</sup> The fast charge thermalization leads to the generation of hot carriers<sup>[33]</sup> upon fs-laser pulses in the presence of oxidative species.<sup>[20]</sup> It plays a major role in carbon lattice engineering during TPO.<sup>[34]</sup>

Raman spectroscopy was used to confirm the TPO process of SWCNT. The spectra were measured for fs-laser processed and non-processed regions of the same nanotube (Figure 1b). The prominent blue shift of the G band and the increase of the D band intensity show the *p*-doping of SWCNT and the defect number growth after fs-laser irradiation<sup>[24,30]</sup>. Further, laser modified FETs were characterized by a semiconductor parameter analyzer. The generated defects also change the electrical properties of the individual SWCNT. Output *I-V* curves (Figure 1c) demonstrate the resistance growth and diode-like characteristic after the laser processing of the channel, while transfer curves (Figure 1d) show the drastic increase of the  $I_{\text{ON}}/I_{\text{OFF}}$  ratio which can be interpreted as an energy band gap increasing in the partly oxidized quasi-metallic nanotube. The changes in electrical characteristics for all devices after TPO are summarized in Table S1, Supporting Information. The conductivity of the SWCNT before fs-

laser oxidation is calculated as  $1.2 \mu\text{S } \mu\text{m}^{-1}$ , and it decreases after the functionalization to  $0.6 \mu\text{S } \mu\text{m}^{-1}$  at  $V_{\text{GS}} = -10 \text{ V}$ .  $Sp^3$  defects could decrease the charge carrier mobility, hence, reducing the conductivity. Additionally, atomic force microscopy (AFM) images of SWCNT (Figure S4, Supporting Information) indicate that the change occurs in local inelastic properties of the processed nanotube compared with the pristine one.

## 2.2. Characterization of a TPO planar junction in SWCNT transistors

Local TPO of our SWCNT FETs results in a bandgap opening in initially qm-SWCNT, and alteration of the morphology of the irradiated region of SWCNT along with the elastic properties change compared with a pristine part of the same nanotube. Taking a closer look at the processed SWCNT FETs, we found out that there is a good correlation between AFM image and Raman mapping of SWCNT with a planar junction in the nanotube (**Figure 2a-d**, Figure S5 and S6, Supporting Information). Figure 2a shows no visible changes in morphology with the only increase of the height up to  $\sim 0.5 \text{ nm}$  in the irradiated part. The latter could be attributed to grafted oxygen groups and the absorbance of water molecules in the area of laser processing. The Raman map shows the rise of the D band in the processed regions of SWCNT (Figure 2c,d, Figure S6, Supporting Information). The blueshift and a slight decrease of the G band intensity (Figure 2c,e) indicate the oxidation and doping of the carbon nanotube previously observed for a local TPO.<sup>[15]</sup> However, the rise of the D band intensity and the defect concentration (Figure 2f) were not confirmed by previous observations that could be attributed to the different levels of oxidation. The defect density can be locally altered up to  $10^{12} \text{ cm}^{-2}$  with a preserved integrity of a hexagonal lattice of a nanotube. These changes coincide with our previous results for graphene functionalization via fs-laser pulses,<sup>[28,32]</sup> where we demonstrated that the majority of the defects are oxygen groups, especially epoxy groups, which were grafted to the surface via TPO. **Note that during TPO the oxidative groups tend to organize clusters rather than scatter<sup>29</sup> that can increase the local defect density near the planar junction.** In this study, we suggest that the oxidation of the

SWCNT opens the energy gap by raising the charge traps near the nanotube.<sup>[25]</sup> Thus, a planar junction is formed in a single SWCNT due to the opening/widening of the energy gap in its part. Compared to continuous wave laser-induced photooxidation of SWCNT, the fs-laser induced oxidation is non-selective to the conductivity type and the processing of the qm-SWCNT and sc-SWCNTs gives similar results.<sup>[23]</sup> It is due to the excited electrons that stay hot sufficiently long to be transferred to oxygen molecules and generate reactive oxygen species.

Next, we address the changes in the electrical properties of the fs-laser irradiated SWCNT FETs. We have found a drastic alteration in rectification properties of individual nanotubes after TPO, which indicates the formation of an energy barrier between pristine and functionalized areas. A low level of the saturation current at reversed bias is visible at different temperatures. While at room temperature the saturation current slightly increases with negative bias voltage due to the resistive heating, at lower temperatures it is constant. At room temperature the rectification ratio of the fs-laser processed qm-SWCNT is close to  $10^3$  at  $V_{DS} = \pm 2$  V and slightly changes for 150 and 80 K (**Figure 3a**). The measurements at low temperatures reveal the rise of the energy barrier height of the planar junction. When we cool the samples down to 80 K, the conductivity falls, and we observe a significant shift in the diode threshold voltage ( $V_T$ ) (**Figure 3a**). The  $V_T$  shifts to higher values (0.9 V at 80 K) compared to 0.1 V at room temperature<sup>[35,36]</sup>, and conductance falls due to the reduction of the free charge carriers concentration.<sup>[37]</sup>

The conductivity of the TPO nanotube highly depends on the field from the gate, and the  $I_{SD}$ - $V_{GS}$  curves demonstrate typical *p*-type behavior (**Figure 3b**). The hysteresis in transfer curves can be explained by the charge transfer to the trapped states in the substrate and water molecules near the nanotube channel that correlates with previously reported results for FETs with aerosol deposited SWCNT.<sup>[38,39]</sup> In our case, the additional trapped states are located on functional oxygen groups. After placing devices in a vacuum, the hysteresis drastically

decreases (Figure S7, Supporting Information). It almost disappears at 80 K (Figure 3b) due to the decrease in the number of active charge traps in the substrate and the redistribution of the adsorbed molecules. The  $I_{ON}/I_{OFF}$  ratio of processed SWCNT slightly increases at lower temperatures due to the total depletion of the impurity states in the energy band and is similar to the ratio of the pristine sc-SWCNT (Figure S8, Supporting Information).  $I$ - $V$  curves for other irradiated structures measured at room temperature are shown in Figure S9, Supporting Information.

Further, we discuss possible mechanisms of the energy barrier formation in the junction between TPO-SWCNT and pristine qm-SWCNT as well as between TPO-SWCNT and metal contact. First, the formation of a type I heterojunction (straddling gap) between the wider bandgap and the smaller one with both p-type doped parts of a nanotube is possible (**Figure 4a**); however, the energy gap of qm-SWCNT is close to zero at room temperature. When we oxidize SWCNT and dope it with holes, we change the charge concentration in TPO-SWCNT and shift down the Fermi level, and, therefore, increase the work function of a nanotube<sup>[40]</sup> as well as the Schottky barrier with a contact. Titanium typically forms the Schottky barrier with SWCNT<sup>[36,41]</sup> due to the low work function in metal (4.3 eV for Ti) compared with a carbon nanotube,<sup>[42]</sup> which is equal to 4.6-4.8 eV. Second, the transition of the band profile from pure  $p$ - $p$  to  $p$ - $p^+$  leads to the Fermi level pinch at the boundary between TPO-SWCNT and qm-SWCNT, and TPO-SWCNT and Ti contact, which prevents holes generation and transport to the opposite electrode.<sup>[10]</sup> This results in asymmetric  $I$ - $V$  curves of a diode-like type (Figure 3a). However, we should note that the doping effect in a planar junction is rather small and does not cause a significant rise in the energy barrier in the contact between a nanotube and Ti. The presence of the interfacial states associated with trapped states in the substrate also affects the band bending in the planar junction. When there are no dangling bonds in carbon lattice and oxygen covers the surface uniformly, the smooth type I heterojunction is possible.<sup>[43]</sup> Another viable electronic structure model could be the formation of potential

valleys induced by single scattered defects.<sup>[44]</sup> Still, the energy bandgap opening is not followed by this model, only if a periodic structure is formed on the surface.

The obvious decrease of the hysteresis with temperature due to the less amount of trapped states in the substrate and on functional oxygen groups, and almost the same level of the saturation current at high negative gate voltages for all measured temperatures, have a good agreement with the model of the Schottky barrier formation. The tunneling mechanism is prevailing for a high gate voltage amplitude and weakly depends on temperature, while for the low amplitude of  $V_{GS}$ , the thermal emission has a major impact.<sup>[45,46]</sup> Additionally, we observe the increase of the current at high positive gate voltages, when the temperature falls, which is related to a higher emission probability of the electrons from the traps.<sup>[47]</sup> Using the equations for the ideal Schottky barrier<sup>[48]</sup> (1) and the bias-dependent Schottky barrier height (2) we can estimate the Schottky barrier height  $\Phi_{b0}$  as  $\sim 60$  mV at  $V_{DS} = 0$  V for the TPO junction in SWCNT (see Figure 4b,c), which is quite low.<sup>[49]</sup>

$$I \sim T^2 \exp\left(-\frac{e\Phi_b}{kT}\right) \quad (1)$$

$$\Phi_b = \Phi_{b0} - \left(\frac{eV}{\pi\epsilon\epsilon_0}\right)^{\frac{1}{2}} \quad (2)$$

The conditions of the non-ideal diode should be applied for more accurate calculations. Thus, we can conclude that the doping of CNT by grafted oxygen species drastically changes the morphology, optical, and electrical properties of SWCNT and leads to the formation of a diode-type planar junction.

### 2.3. Ultrahigh Photosensitivity of SWCNT with planar junction

The fabricated planar junctions in SWCNT via fs-laser irradiation exhibit a notable photocurrent ( $I_{ph}$ ) in the measured optical range at low light intensities. We measured the responsivity and the external quantum efficiency (EQE) (Figure S10, Supporting Information) in the range from 350 nm to 1000 nm using a xenon lamp and a monochromator (**Figure 5a**).

The samples show a noticeable increase of photoresponsivity compared with pristine SWCNT. Three LEDs were used to carefully measure the sensitivity of the SWCNT to light at several wavelengths, namely 470 nm, 590 nm, and 630 nm. The current was measured as a function of bias under the illumination of the whole FET with an incident power of  $400 \mu\text{W cm}^{-2}$  (Figure 5b). The  $I_{\text{ph}}$  is larger under forward bias ( $V_{\text{DS}} = 1 \text{ V}$ ) than under reverse bias ( $V_{\text{DS}} = -1 \text{ V}$ ). The electrical characteristics in the dark and upon illumination for four additional transistors are shown in Figure S11, Supporting Information. The parameters of irradiation highly affect the properties of a planar junction in SWCNT. The calculated responsivities for SWCNT FETs at three wavelengths are shown in Figure 5c (forward bias) and Figure S12, Supporting Information (reverse bias). The largest photoresponsivity was found for 470 nm light in a good correlation with the broadband responsivity graph. Moreover, the photoresponse could be increased by applying the gate voltage (Figure 5d). Gate-dependent photosensitivity in the fabricated FETs are explained by the bandgap renormalization with the increase of the gate voltage.<sup>[50]</sup> This helps to overcome the charge traps switching and should improve the temporal characteristics of the phototransistor.

For TPO structures, we found a significant rise of the current upon 470 nm LED illumination in a wide temperature range (Figure 6, and Figure S11a-f, Supporting Information). We controlled the light intensity by adjusting the voltage applied to an LED and measured illumination power with a power meter. We found that the  $I_{\text{ph}}$  rises with the light power increase for forward and reverse diode directions (Figure 6a, b). Upon illumination, the current increases up to three orders of magnitude. Additionally, we observe the broadening of the hysteresis in transfer characteristics under LED irradiation (Figure 6d, c) that is especially pronounced at 150 K. The ambipolar behavior is visible for transfer curves at low temperatures, but the current generation in the  $n$ -type regime is weak since there are fewer minority carriers (Figure 6d).

The photoresponsivity of fabricated SWCNT FETs was calculated at different power densities of 470 nm light and at different temperatures (Figure S13, Supporting Information). If we recalculate the responsivity per single SWCNT taking the square of the active area as the distance between electrodes per half of the diode wavelength, we obtain the values over  $2 \cdot 10^7$  A W<sup>-1</sup> for CNT3 at the incident power density of 470 nm light equal to  $5 \mu\text{W cm}^{-2}$ . In Table 1, we compare the responsivity of our devices to those of previously reported individual SWCNT-based photodetectors. Though, it still has low efficiency because the TPO does not provide the precise interface in the junction of modified and non-modified regions. Nevertheless, we demonstrate one of the highest responsivities to ultralow light intensities due to the changes in intrinsic chemical properties of an individual nanotube detector that could be perspective for integrated optoelectronic devices fabrication with high precision. For comparison, we study the photoresponse of the pristine sc-SWCNT grown on the same substrate. Non-modified sc-SWCNT demonstrates a weak photoresponse under the same conditions (Figure S8c). This refers to low photoconductivity of the pristine sc-nanotube that is due to resonance with energetic states in the SWCNT, which located in IR region.<sup>[51]</sup>

#### **2.4. The mechanisms of photocurrent generation in SWCNT planar junction**

Two main mechanisms can give rise to the current generation in fabricated SWCNT FETs upon irradiation. The first one is the photothermoelectric effect, originating from different Seebeck coefficients in pristine and modified parts of a nanotube, as was previously shown for graphene photodetector.<sup>[32]</sup> The second one is the photovoltaic effect arising from the formation of an intramolecular planar junction between the modified and pristine part of SWCNT, which is responsible for a non-linear behavior of the output *I-V* curves. The parasitic electrostatic gating by the trapped charges in the substrate near the modified nanotube could also affect the generated charges under the light.<sup>[52]</sup> In a high vacuum and at

low temperatures, we drastically decrease the number of the charge traps raised for both nanotube interface (adsorbed molecules) and substrate surface.<sup>[47]</sup>

The oxidation of a part of a nanotube leads to a built-in electric field generation in the area of a planar junction. The recent works demonstrate that in  $p$ - $n$  and  $p$ - $p^+$  junctions both mechanisms of the photothermoelectric and photovoltaic current generation are possible, and the dominating mechanism depends on the doping profile.<sup>[9]</sup> In this work, the generated excitons are separated by a built-in electric field and raise the current with the same sign as dark current. The measured  $I_{ph}$  for various wavelengths (Figure 5b) and at different power (Figure S11, Supporting Information) show that the thermoelectric effect is not the main mechanism of the photoresponse. We assume that the slight decrease of the responsivity (Figure 5c) at longer wavelengths (570 nm and 630 nm) compared with 470 nm at the same light intensity and almost constant dark current at 300 and 150 K prove that the photovoltaic effect dominates over photothermoelectric in the SWCNT junction. Under forward bias, the increase of the built-in electric field initiates the rise of the current. Under light irradiation, the photocurrent originates due to the excitons generation in the junction. When the backward voltage is applied (negative in diode), the built-in electric field vanishes, and only high-intensity photons in resonance with excitation bands in oxidized nanotube can generate a relatively small photocurrent in a junction. The increase of the photoresponse at long wavelengths for several TPO processed devices (Figure 5c) can be related to the heating effects in the junction.<sup>[53]</sup>

The transconductance does not change with the gate  $V_T$  shift even at higher light intensities, which indicates that the mobility of the main charge carries is not altered. The gating effect from charge traps changes only the concentration of the main charge carries and does not inject any additional charges. When the nanotube is supported on a substrate, the role of the trapped states in photoinduced charge transfer cannot be neglected.<sup>[54]</sup> For a high vacuum and

low temperatures, we can partly reduce the water impact leaving the surface trap states near the nanotube.

## 2.5. The analysis of the operation speed of SWCNT FETs

Upon light illumination, the photogenerated holes in a nanotube are trapped, acting like a positive gate bias leading to the increase of the electron concentration and to a negative shift of the transfer curves, as shown in Figure 6d. In order to study the underlying photodetection mechanism and effect of traps on the photovoltaic response, we measure the response times of the device (**Figure 7**). The measurements were performed under standard conditions upon fs-laser irradiation at the energies below the TPO process and upon 470 nm LED illumination to compare both the activation and relaxation mechanisms. The response to fs-laser and LED irradiation are shown in Figure 7a and 7b, respectively. The trapped charges increase the time constants of photoresponse in a nanotube. For fs pulse illumination, we observe the reversible decrease in current that was also observed for non-processed SWCNT at the laser energies below TPO that can be explained by induced electrostatic doping<sup>[52,55]</sup> by activated localized charge traps in the substrate. The device exhibits a negative and fast photoresponse in Figure 7a while it shows a positive but slower photoresponse in Figure 7b. The fast photoresponse to the fs pulse demonstrates the rise faster than the resolution of our measuring setup (limited to 3 ms) and a decay time of 0.318 s. As far as fs pulses generate high-energy electrons (hot electrons), some of them can be trapped, attracting the holes in the channel and thus decreasing the current. This effect is low due to the limited number of electrons that can be thermalized during the fs pulse, and the restoration of characteristics goes rapidly. When the higher energy pulses are applied, we increase the current through the energy barrier in the junction. The rise time is swift and corresponds to the electron-hole generation and transfer from the barrier by the built-in electric field. The trapped holes attract electrons, increasing the number of holes in the channel. Two decay timescales are clearly distinguished: fast in the

range of few seconds and slow in the range of hundred seconds. During decay, electron-hole recombination results in the rapid component and is followed by the slow one due to the discharging of trap states.<sup>[56]</sup> The longer releasing is due to the oxidized nanotubes that can attract more states from surroundings under normal conditions, also explaining the transfer characteristic hysteresis increasing in a vacuum at low temperatures upon illumination. Thus, we have two mechanisms affecting the photoresponse of our devices, the photovoltaic effect in the barrier of a nanotube junction (fast) and photogating from trapped charges (slow). We measured fifteen devices with TPO processed nanotubes at different energies resulting in various levels of SWCNT oxidation. All of them show similar output and transfer characteristics upon light illumination. Moreover, few transfer characteristics demonstrate a competitive effect in photogating and photovoltaic depending on the increase of the LED power that can be attributed both to the intrinsic difference of pristine nanotubes and the level of oxidation (Figure S11o,r, Supporting Information). Therefore, the further improvement of the direct laser writing methods of a nanotube bandgap engineering and systematic study of a correlation of laser processing with functional properties of nanotube-based devices should be made for a better understanding of charge transfer in such type of devices with an intramolecular junction. The possible injection of the charge carriers to the deep traps in the substrate formed during the fs-laser processing of a nanotube should also affect the transport properties. But they are not changing the photoresponse according to small-time constants in developed devices.

The suggested technology of maskless local patterning of electronic and optical properties can be further designed by laser processing beyond the diffraction limit (like STED), providing high-density integration of CMOS-compatible devices for developed logic circuits,<sup>[57]</sup> photonic interconnections<sup>[3]</sup> as well as optical synapsis.<sup>[58]</sup>

### 3. Conclusion

In summary, we demonstrate, for the first time, the facile method of a planar junction formation in SWCNT by the local two-photon oxidation using fs-laser irradiation and study of its electrical and optoelectronic properties. Varying the power and number of pulses per  $\mu\text{m}^2$ , we can control the level of oxidation and photoresponse of fabricated devices. The bandgap opening for a processed part of CNT is caused by an attachment of functionalized groups and the formation of  $sp^3$  defects. The rectification properties of a junction were studied at different temperatures demonstrating the presence of a tunable barrier. These features were utilized to gain a high photoresponse in a broadband range for SWCNT planar junctions, which originates from the interplay between the photovoltaic and photogating effects.

The novel technology provides an effective route for ultralow light intensity detection in a wide temperature range with unique single-SWCNT planar junctions. The method of local ultrafast photooxidation presents a versatile approach compatible with standard CMOS technology for a planar junction formation with engineered electrical and optical properties, which can be further applied for novel type of functional electronic and photonic devices.

#### 4. Experimental Section

*Fabrication of Individual SWCNT FETs:* SWCNT were grown by gas-phase formation based on the thermal decomposition of ferrocene in the presence of carbon monoxide<sup>[59]</sup> and directly deposited onto a cold highly doped ( $p^{++}$ ) 100 mm Si wafer with 300 nm thermal  $\text{SiO}_2$  at the same time. The density of carbon nanotubes on the surface was  $\sim 1$  nanotube per  $10 \mu\text{m}^2$ . Source and drain 100/15 nm Au/Ti electrodes were fabricated by a photolithographic lift-off process, the gate electrode was  $p^{++}$  Si substrate. The distance between source and drain contacts was  $1.5 \mu\text{m}$ , the oxide layer was 300 nm thick. The fabrication route and scanning electron microscopy (SEM) images of SWCNT FETs are shown in Figure S1, Supporting Information. Moreover, to visualize the morphology and structural changes after fs-laser processing, SWCNT FETs with a source-to-drain distance of  $12 \mu\text{m}$  were made. The substrate

was scribed to isolate devices with a  $2 \text{ mm}^2$  area. Further, chips were washed in boiled acetone to remove the photoresist and heated at  $250 \text{ }^\circ\text{C}$  in a high vacuum to eliminate the organic residuals. In this work, we study 17 different FETs which channels are individual quasi-metallic and semiconducting nanotubes (Table S1, Supporting Information).

*Device Characterization:* SWCNT samples were characterized via AFM (Solver Pro (NT-MDT, Russia)) and SEM (HITACHI S-4800 II (HITACHI, Japan)). The additional nanotubes in the channel, if present, were ablated by fs-laser. The output and transfer I-V curves were measured by a semiconductor parameter analyzer (MNIPI, Belarus) and a home-made measurement board. Temperature measurements were performed using the cryostat and liquid nitrogen to cool devices to  $77 \text{ K}$ . Raman spectra were carried out on micro-Raman spectrometer Centaur HR (Nanoscan Technology, Russia) with a  $\times 100$  objective at  $532 \text{ nm}$  (Cobolt, Sweden) with a beam spot of  $\sim 1 \mu\text{m}^2$  and laser power of  $0.5 \text{ mW}$ .

*Femtosecond Laser Processing:* SWCNT FETs were placed on the motorized XY stage, the galvoscaner (Newson, Belgium) was fixed on a vertical precision stage (Aerotech, USA) for adjustment of the focal position. The fs-laser (Satsuma HP2, Amplitude Systems, France) emitting at  $515 \text{ nm}$  was used to process the SWCNT (Figure S2, Supporting Information) with the following parameters:  $280 \text{ fs}$  pulse duration, varied pulse energy in the range of  $0.5\text{-}6 \text{ nJ}$ ,  $500 \text{ kHz}$  repetition rate. The pulse energy was far below the ablation threshold for SWCNT, which was estimated as  $13 \text{ nJ}$ . The accumulated dose for a nanotube at certain pulse energy varied via the scanning speed, i.e., the number of pulses per  $\mu\text{m}^2$ .

*Photoresponse measurements:* Continuous-wave  $470 \text{ nm}$ ,  $590 \text{ nm}$ , and  $630 \text{ nm}$  LEDs (ThorLabs, USA) with a maximum power density of  $5 \text{ mW cm}^{-2}$  were used to conduct photocurrent experiments. The measurements of time response were performed via the previously mentioned fs-laser at the energies below SWCNT photooxidation and  $470 \text{ nm}$  LED. To measure external quantum efficiency and responsivity in the range of  $350\text{-}1000 \text{ nm}$ ,

we used IL75E xenon lamp (Bentham, UK) with a chopper at 1 kHz and SID-101 monochromator with a 600 lines/mm grating (Photon Technologies International, USA).

### Supporting Information

Supporting Information is available from the Wiley Online Library or from the author.

### Acknowledgements

This research was supported by a Russian Science Foundation project No.19-19-00401 (experiment design, fabrication, and characterization of functionalized carbon nanotube photodetectors) and in part by Russian Foundation of Basic Research projects No. 20-03-00804 (synthesis of carbon nanotubes) and No. 18-29-20116 (low-temperature experiments). The authors thank Dr. A. Bakulin at Imperial College London for access to and assistance with EQE measurements, I.A. Gayduchenko at Moscow State Pedagogical University for helping with low-temperature experiments, and N.G. Kokareva at Moscow State University for assistance with fs-laser processing.

### Conflict of Interest

The authors declare no conflict of interest.

Received: ((will be filled in by the editorial staff))

Revised: ((will be filled in by the editorial staff))

Published online: ((will be filled in by the editorial staff))

### References

- [1] M. M. Waldrop, *Nature* **2016**, *530*, 144.
- [2] C. Sun, M. T. Wade, Y. Lee, J. S. Orcutt, L. Alloatti, M. S. Georgas, A. S. Waterman, J. M. Shainline, R. R. Avizienis, S. Lin, B. R. Moss, R. Kumar, F. Pavanello, A. H. Atabaki, H. M. Cook, A. J. Ou, J. C. Leu, Y.-H. Chen, K. Asanović, R. J. Ram, M. A. Popović, V. M. Stojanović, *Nature* **2015**, *528*, 534.
- [3] Y. Liu, S. Wang, H. Liu, L.-M. Peng, *Nat. Commun.* **2017**, *8*, 15649.
- [4] A. Riaz, A. Alam, P. B. Selvasundaram, S. Dehm, F. Hennrich, M. M. Kappes, R. Krupke, *Adv. Electron. Mater.* **2019**, *5*, 1800265.
- [5] H. Fang, P. Wu, P. Wang, Z. Zheng, Y. Tang, J. C. Ho, G. Chen, Y. Wang, C. Shan, X. Cheng, J. Zhang, W. Hu, *Adv. Opt. Mater.* **2019**, *7*, 1900597.

- [6] Y. Chen, G. Royal, E. Flahaut, S. Cobo, V. Bouchiat, L. Marty, N. Bendiab, *Adv. Mater.* **2017**, *29*, 1605745.
- [7] X. He, F. Léonard, J. Kono, *Adv. Opt. Mater.* **2015**, *3*, 989.
- [8] M. Barkelid, V. Zwiller, *Nat. Photonics* **2014**, *8*, 47.
- [9] G. Buchs, S. Bagiante, G. A. Steele, *Nat. Commun.* **2014**, *5*, 4987.
- [10] G. Buchs, M. Barkelid, S. Bagiante, G. A. Steele, V. Zwiller, *J. Appl. Phys.* **2011**, *110*, 074308.
- [11] S.-W. Chang, J. Theiss, J. Hazra, M. Aykol, R. Kapadia, S. B. Cronin, *Appl. Phys. Lett.* **2015**, *107*, 053107.
- [12] L. Aspirtarte, D. R. McCulley, E. D. Minot, *Nano Lett.* **2016**, *16*, 5589.
- [13] C. Chen, C. Song, J. Yang, D. Chen, W. Zhu, C. Liao, X. Dong, X. Liu, L. Wei, N. Hu, R. He, Y. Zhang, *Nano Energy* **2017**, *32*, 280.
- [14] G. Fedorov, A. Kardakova, I. Gayduchenko, I. Charayev, B. M. Voronov, M. Finkel, T. M. Klapwijk, S. Morozov, M. Presniakov, I. Bobrinetskiy, R. Ibragimov, G. Goltsman, *Appl. Phys. Lett.* **2013**, *103*, 181121.
- [15] J. Aumanen, A. Johansson, O. Herranen, P. Myllyperkiö, M. Pettersson, *Phys. Chem. Chem. Phys.* **2015**, *17*, 209.
- [16] T. Kato, R. Hatakeyama, J. Shishido, W. Oohara, K. Tohji, *Appl. Phys. Lett.* **2009**, *95*, 083109.
- [17] T. Shiraishi, G. Juhász, T. Shiraki, N. Akizuki, Y. Miyauchi, K. Matsuda, N. Nakashima, *J. Phys. Chem. C* **2016**, *120*, 15632.
- [18] G. Buchs, D. Bercioux, L. Mayrhofer, O. Gröning, *Carbon* **2018**, *132*, 304.
- [19] Z. Yao, H. W. C. Postma, L. Balents, C. Dekker, *Nature* **1999**, *402*, 273.
- [20] L. M. Gomez, A. Kumar, Y. Zhang, K. Ryu, A. Badmaev, C. Zhou, *Nano Lett.* **2009**, *9*, 3592.

- [21] C.-W. Lin, S. M. Bachilo, Y. Zheng, U. Tsedev, S. Huang, R. B. Weisman, A. M. Belcher, *Nat. Commun.* **2019**, *10*, 2874.
- [22] D. Asheghali, P. Vichchulada, M. D. Lay, *J. Am. Chem. Soc.* **2013**, *135*, 7511.
- [23] S. Yasuda, T. Yoshii, S. Chiashi, S. Maruyama, K. Murakoshi, *ACS Appl. Mater. Interfaces* **2017**, *9*, 38992.
- [24] I. I. Bobrinetskiy, A. V. Emelianov, N. Otero, P. M. Romero, *Appl. Phys. Lett.* **2015**, *107*, 043104.
- [25] J. Chen, R. Dhall, B. Hou, S. Yang, B. Wang, D. Kang, S. B. Cronin, *Appl. Phys. Lett.* **2016**, *109*, 153109.
- [26] J. M. Simmons, B. M. Nichols, S. E. Baker, M. S. Marcus, O. M. Castellini, C.-S. Lee, R. J. Hamers, M. A. Eriksson, *J. Phys. Chem. B* **2006**, *110*, 7113.
- [27] M. E. Mendoza, E. H. M. Ferreira, A. Kuznetsov, C. A. Achete, J. Aumanen, P. Myllyperkiö, A. Johansson, M. Pettersson, B. S. Archanjo, *Carbon* **2019**, *143*, 720.
- [28] I. Bobrinetskiy, A. Emelianov, A. Nasibulin, I. Komarov, N. Otero, P. M. Romero, *J. Phys. D. Appl. Phys.* **2016**, *49*, 41LT01.
- [29] J. Koivistoinen, L. Sládková, J. Aumanen, P. Koskinen, K. Roberts, A. Johansson, P. Myllyperkiö, M. Pettersson, *J. Phys. Chem. C* **2016**, *120*, 22330.
- [30] J. Aumanen, A. Johansson, J. Koivistoinen, P. Myllyperkiö, M. Pettersson, *Nanoscale* **2015**, *7*, 2851.
- [31] A. Johansson, H.-C. Tsai, J. Aumanen, J. Koivistoinen, P. Myllyperkiö, Y.-Z. Hung, M.-C. Chuang, C.-H. Chen, W. Y. Woon, M. Pettersson, *Carbon* **2017**, *115*, 77.
- [32] A. V. Emelianov, D. Kireev, A. Offenhäusser, N. Otero, P. M. Romero, I. I. Bobrinetskiy, *ACS Photonics* **2018**, *5*, 3107.
- [33] Y.-Z. Ma, J. Stenger, J. Zimmermann, S. M. Bachilo, R. E. Smalley, R. B. Weisman, G. R. Fleming, *J. Chem. Phys.* **2004**, *120*, 3368.

- [34] R. K. Raman, Y. Murooka, C.-Y. Ruan, T. Yang, S. Berber, D. Tománek, *Phys. Rev. Lett.* **2008**, *101*, 077401.
- [35] M. H. Yang, K. B. K. Teo, W. I. Milne, D. G. Hasko, *Appl. Phys. Lett.* **2005**, *87*, 253116.
- [36] H. M. Manohara, E. W. Wong, E. Schlecht, B. D. Hunt, P. H. Siegel, *Nano Lett.* **2005**, *5*, 1469.
- [37] M. Nygard, J., Cobden, D., Bockrath, *Appl Phys A* **1999**, *69*, 297.
- [38] M. Y. Timmermans, K. Grigoras, A. G. Nasibulin, V. Hurskainen, S. Franssila, V. Ermolov, E. I. Kauppinen, *Nanotechnology* **2011**, *22*, 065303.
- [39] M. Y. Timmermans, D. Estrada, A. G. Nasibulin, J. D. Wood, A. Behnam, D. Sun, Y. Ohno, J. W. Lyding, A. Hassanien, E. Pop, E. I. Kauppinen, *Nano Res.* **2012**, *5*, 307.
- [40] R. A. Hatton, N. P. Blanchard, L. W. Tan, G. Latini, F. Cacialli, S. R. P. Silva, *Org. Electron.* **2009**, *10*, 388.
- [41] P. Wilhite, A. A. Vyas, J. Tan, J. Tan, T. Yamada, P. Wang, J. Park, C. Y. Yang, *Semicond. Sci. Technol.* **2014**, *29*, 054006.
- [42] A. P. Tsapenko, A. E. Goldt, E. Shulga, Z. I. Popov, K. I. Maslakov, A. S. Anisimov, P. B. Sorokin, A. G. Nasibulin, *Carbon* **2018**, *130*, 448.
- [43] D. S. Kopylova, F. S. Fedorov, A. A. Alekseeva, E. P. Gilshteyn, A. P. Tsapenko, A. V. Bubis, A. K. Grebenko, Z. I. Popov, P. B. Sorokin, Y. G. Gladush, A. S. Anisimov, A. G. Nasibulin, *Nanoscale* **2018**, *10*, 18665.
- [44] X. Ma, L. Adamska, H. Yamaguchi, S. E. Yalcin, S. Tretiak, S. K. Doorn, H. Htoon, *ACS Nano* **2014**, *8*, 10782.
- [45] J. Svensson, E. E. B. Campbell, *J. Appl. Phys.* **2011**, *110*, 111101.
- [46] J. Svensson, A. A. Sourab, Y. Tarakanov, D. S. Lee, S. J. Park, S. J. Baek, Y. W. Park, E. E. B. Campbell, *Nanotechnology* **2009**, *20*, 175204.

- [47] R. S. Park, M. M. Shulaker, G. Hills, L. Suriyasena Liyanage, S. Lee, A. Tang, S. Mitra, H.-S. P. Wong, *ACS Nano* **2016**, *10*, 4599.
- [48] S. M. Sze, *Physics of Semiconductor Devices*; John Wiley & Sons, 1981.
- [49] L. Huang, E. F. Chor, Y. Wu, Z. Guo, *Carbon* **2010**, *48*, 1298.
- [50] K. H. Park, S.-H. Lee, F. Toshimitsu, J. Lee, S. H. Park, F. Tsuyohiko, J.-W. Jang, *Carbon* **2018**, *139*, 709.
- [51] M. Freitag, Y. Martin, J. A. Misewich, R. Martel, P. Avouris, *Nano Lett.* **2003**, *3*, 1067.
- [52] A. Tiberj, M. Rubio-Roy, M. Paillet, J.-R. Huntzinger, P. Landois, M. Mikolasek, S. Contreras, J.-L. Sauvajol, E. Dujardin, A.-A. Zahab, *Sci. Rep.* **2013**, *3*, 2355.
- [53] A. Mahmoudi, M. Troudi, P. Bondavalli, N. Sghaier, *J. Mater. Sci.* **2017**, *52*, 10273.
- [54] S. Pyo, W. Kim, H.-I. Jung, J. Choi, J. Kim, *Small* **2017**, *13*, 1700918.
- [55] Y. D. Kim, M.-H. Bae, J.-T. Seo, Y. S. Kim, H. Kim, J. H. Lee, J. R. Ahn, S. W. Lee, S.-H. Chun, Y. D. Park, *ACS Nano* **2013**, *7*, 5850.
- [56] V. T. Nguyen, W. Yim, S. J. Park, B. H. Son, Y. C. Kim, T. T. Cao, Y. Sim, Y.-J. Moon, V. C. Nguyen, M.-J. Seong, S.-K. Kim, Y. H. Ahn, S. Lee, J.-Y. Park, *Adv. Funct. Mater.* **2018**, *28*, 1802572.
- [57] G. Hills, C. Lau, A. Wright, S. Fuller, M. D. Bishop, T. Srimani, P. Kanhaiya, R. Ho, A. Amer, Y. Stein, D. Murphy, Arvind, A. Chandrakasan, M. M. Shulaker, *Nature* **2019**, *572*, 595.
- [58] Z. Liu, S. Dai, Y. Wang, B. Yang, D. Hao, D. Liu, Y. Zhao, L. Fang, Q. Ou, S. Jin, J. Zhao, J. Huang, *Adv. Funct. Mater.* **2020**, *30*, 1906335.
- [59] A. Moisala, A. G. Nasibulin, D. P. Brown, H. Jiang, L. Khriachtchev, E. I. Kauppinen, *Chem. Eng. Sci.* **2006**, *61*, 4393.

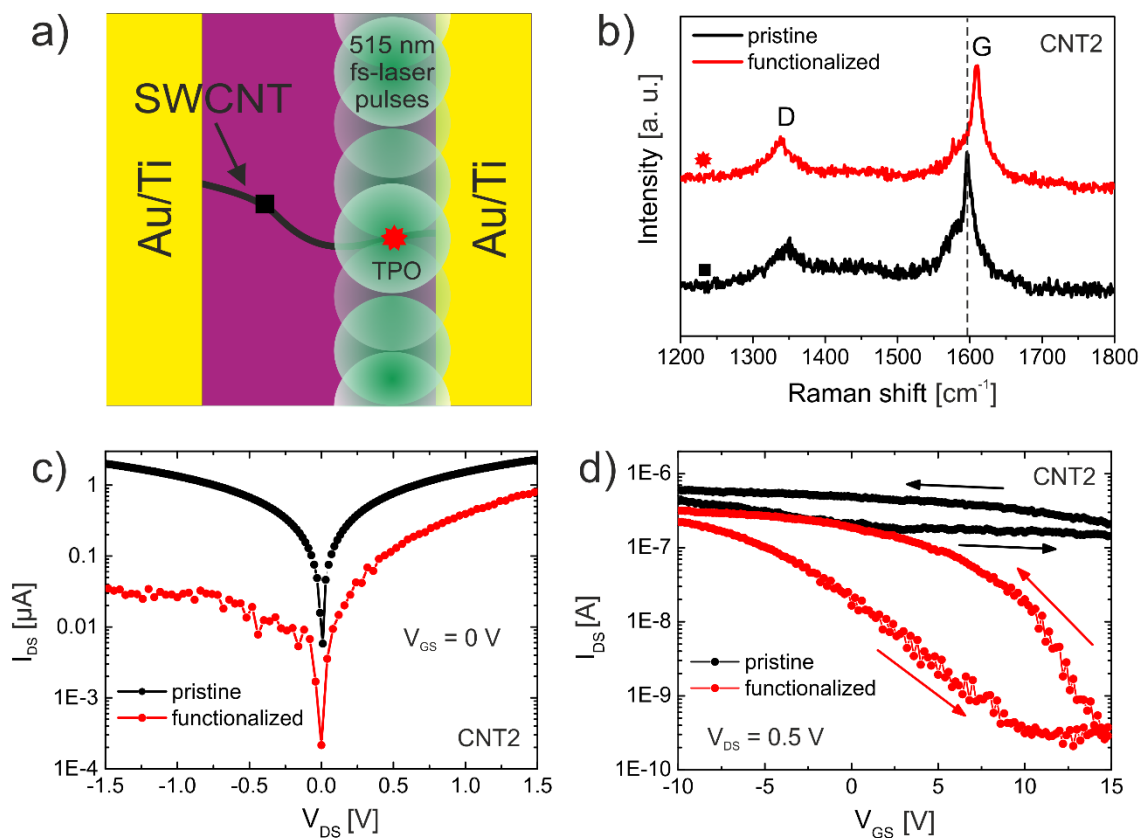


**Figure 1.** Fs-laser processing of the SWCNT FET channel. (a) The schematic image of laser modification of a single SWCNT channel through fs-laser irradiation. (b) Raman spectra for the pristine and laser processed CNT2 (the dotted line shows initial G band position). (c)  $I_{\text{DS}}-V_{\text{DS}}$  curves for the CNT2 before and after laser processing. (d)  $I_{\text{DS}}-V_{\text{GS}}$  curves for the CNT2 before and after laser processing.

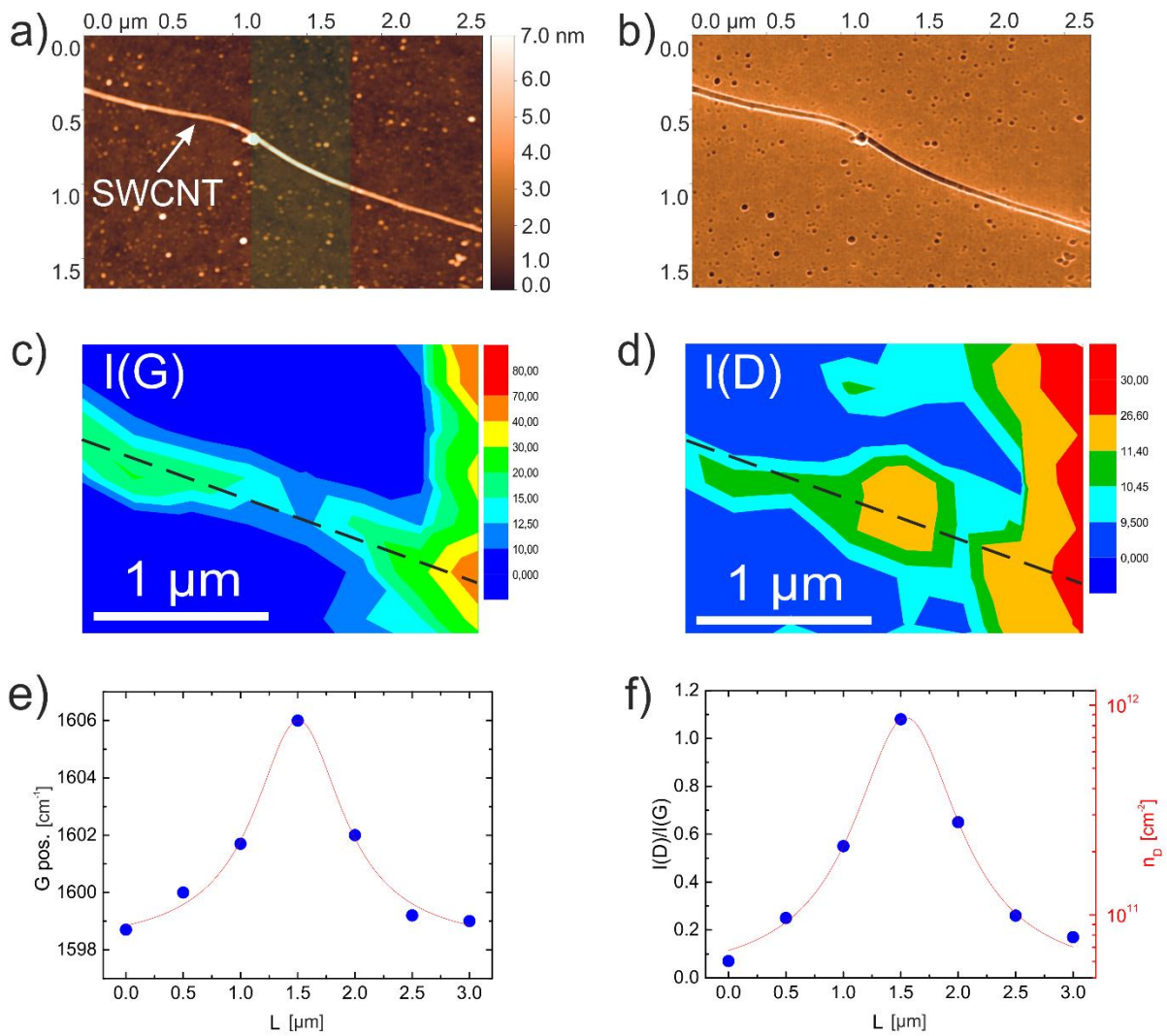


**Figure 2.** Characterization of a planar junction in a carbon nanotube channel formed by fs-laser. (a, b) AFM image of the CNT15 FET: height (a) and cantilever oscillation phase shift (b). (c, d) Raman map for the same area of CNT15 for G (c) and D band (d) intensities. (e, f) The shift of the G band position (e) and defect concentration (f) across the dashed line in (c) and (d), respectively.

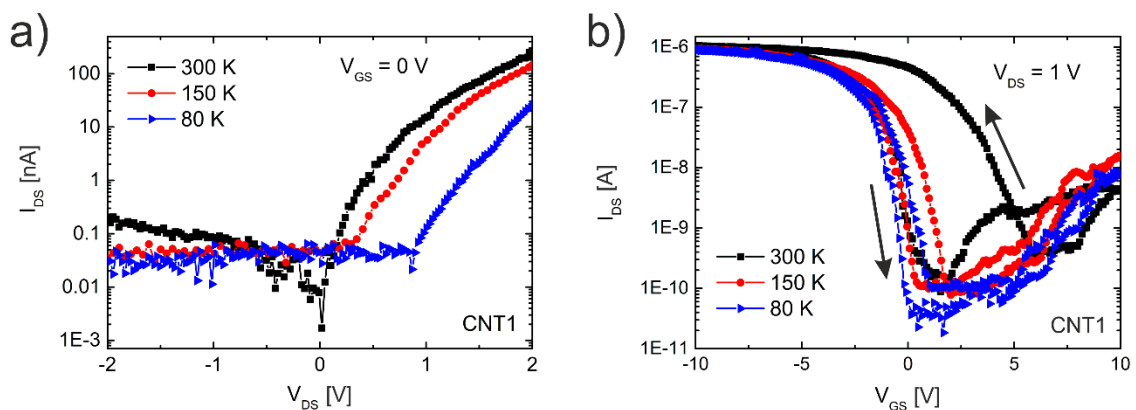


**Figure 3.** Temperature dependence of  $I$ - $V$  characteristics for SWCNT FET. a) Output  $I$ - $V$  curves at 300, 150, and 80 K at  $V_{GS} = 0$  V. b) Transfer  $I$ - $V$  curves at 300, 150, and 80 K at  $V_{DS} = 1$  V.

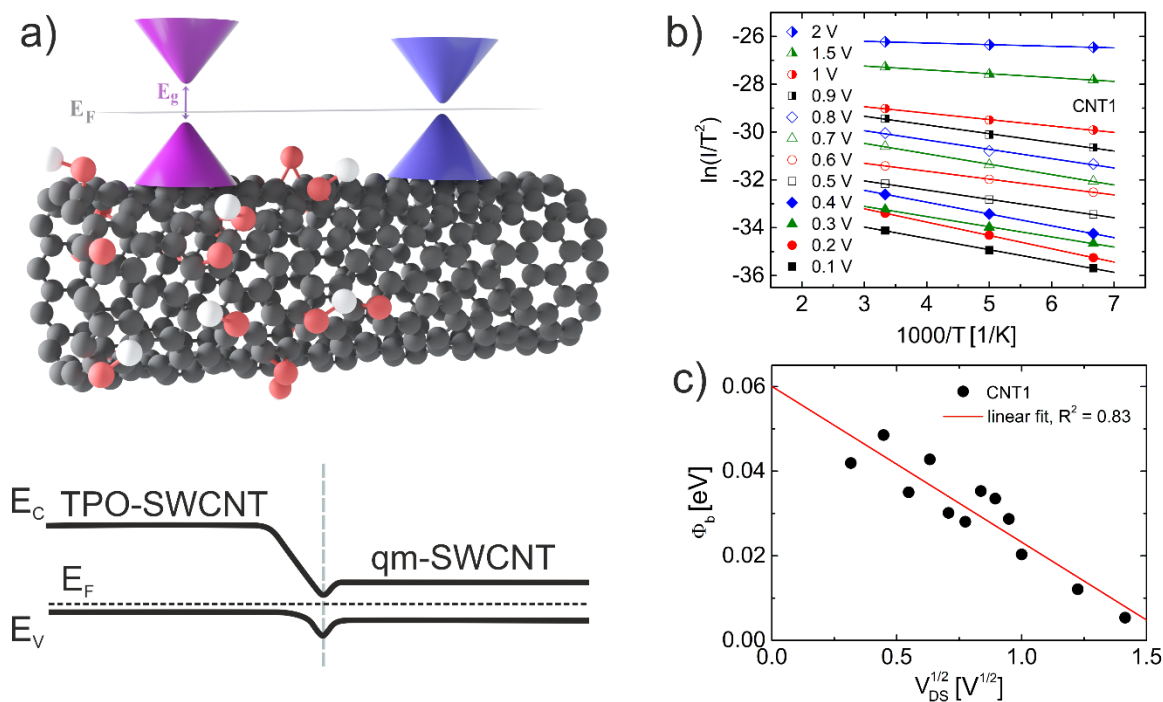


**Figure 4.** The energy barrier formation in a nanotube channel. (a) The scheme of SWCNT doping with oxidative species and the energy band diagram illustrating the planar junction formation between TPO-SWCNT and qm-SWCNT in the presence of interface states (traps). (b) Plots of  $\ln(I/T^2)$  versus  $1/T$  for  $T$  from 150 to 300 K for different bias voltages ( $V_{DS} = 0.1$ –2 V) for CNT1. (c) The biased dependent  $\Phi_b$  is extracted from (b) and plotted as a function of bias voltage ( $V_{DS}^{1/2}$ ) to yield the Schottky barrier height at zero bias voltage  $\Phi_{b0}$ .

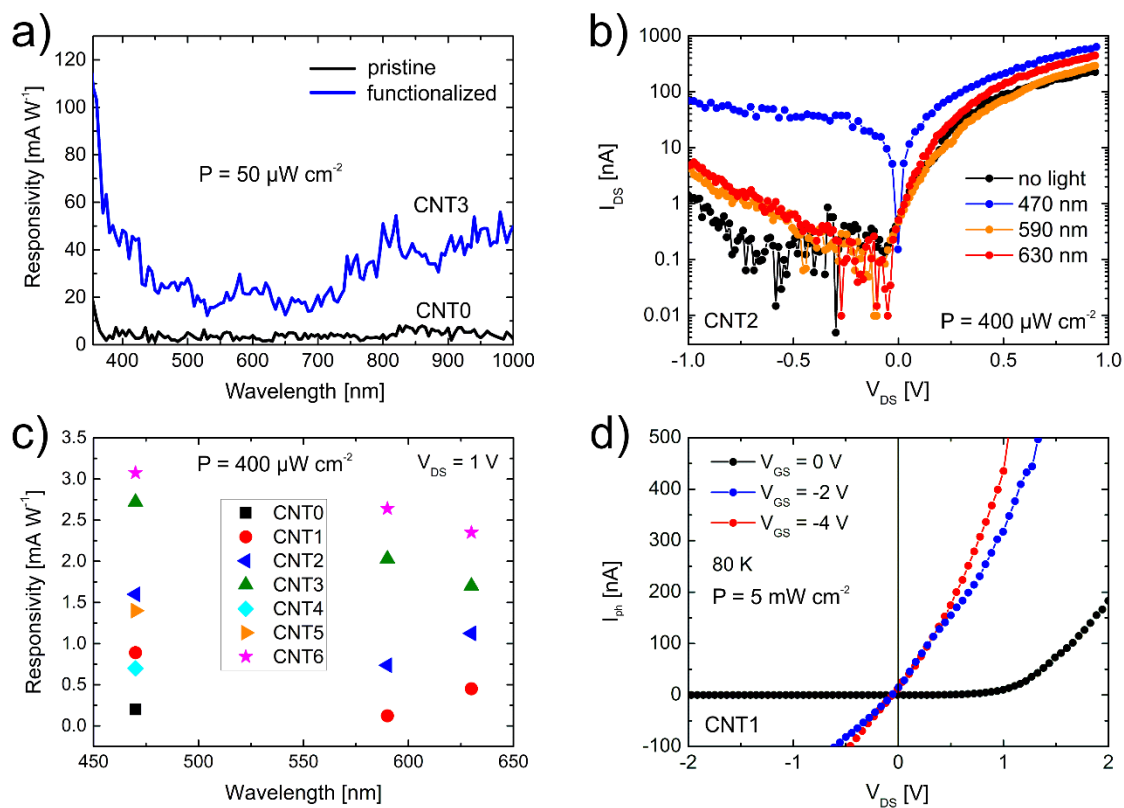


**Figure 5.** The photoresponse of the SWCNT junction at different wavelengths. (a) The responsivity and EQE for pristine and processed SWCNT upon xenon lamp illumination. (b)  $I_{DS}$ - $V_{DS}$  curves at three different wavelengths of the LED light. (c) Photoresponsivity at three different wavelengths at  $V_{GS} = 0$  V and  $V_{DS} = 1$  V. (d) Photocurrent for CNT1 upon 5 mW 470 nm illumination at 0, -2 and -4 V gate voltage at 80 K.

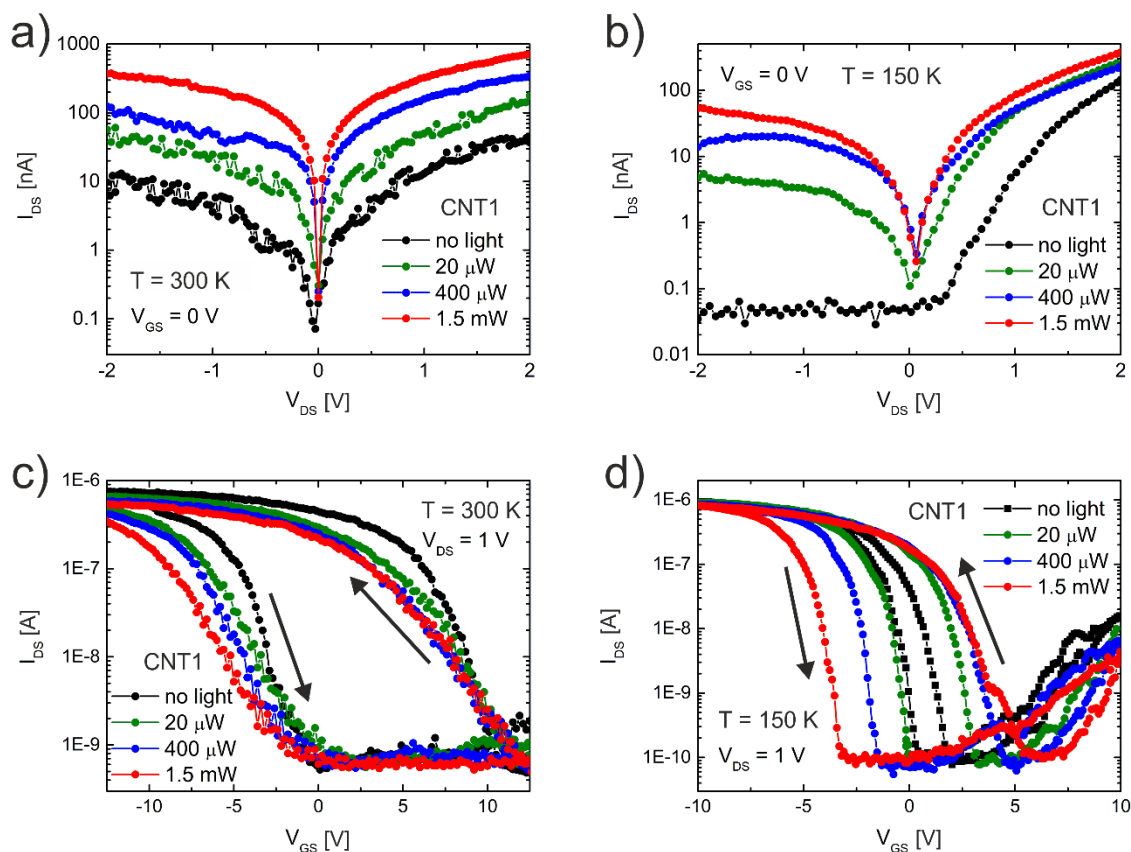


**Figure 6.** Electrical measurements of SWCNT FET upon 470 nm LED illumination. (a) Output  $I$ - $V$  characteristics of the CNT1 under standard conditions (300 K, 1 atm). (b) Output  $I$ - $V$  curves of the CNT1 at 150K and  $5 \cdot 10^{-3}$  Pa. (c) Transfer  $I$ - $V$  characteristics of the CNT1 at standard conditions. (d) Transfer  $I$ - $V$  characteristics of the CNT1 at 150K and  $5 \cdot 10^{-3}$  Pa. The power of 470 nm LED varied from  $20 \mu\text{W cm}^{-2}$  to  $1.5 \text{ mW cm}^{-2}$ .  $V_{DS}$  in (c, d) was set to 1 V.

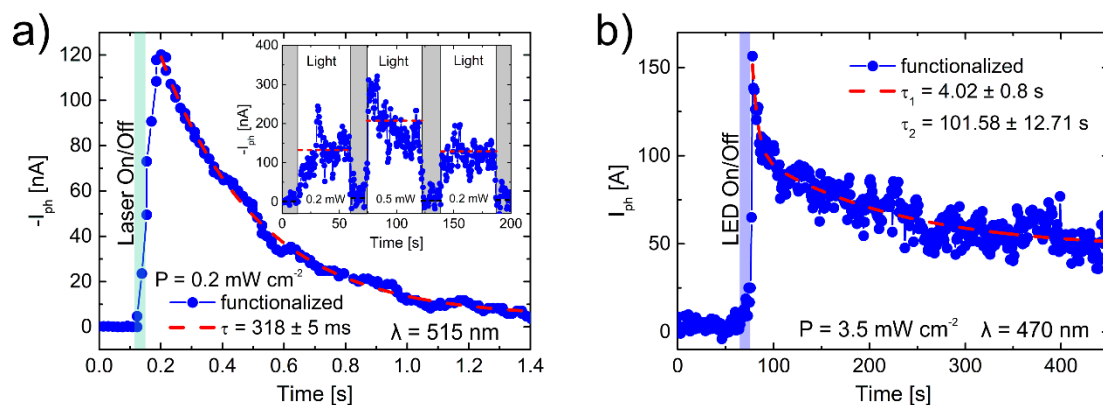


**Figure 7.** Time response of fabricated SWCNT FETs. a) Photoresponse of the CNT2 upon fs-laser pulse with an average power of  $0.2 \text{ mW cm}^{-2}$  at 515 nm. The inset in (a) is a switching of laser pulses between  $0.2 \text{ mW cm}^{-2}$  and  $0.5 \text{ mW cm}^{-2}$ . b) Photoresponse of the CNT2 upon LED On/Off with  $P = 3.5 \text{ mW cm}^{-2}$  and  $\lambda = 470 \text{ nm}$ . The inset in (b) shows the decay of photocurrent with time constants  $\tau_1 = 4.02 \pm 0.8 \text{ s}$  and  $\tau_2 = 101.58 \pm 12.71 \text{ s}$ .

LED illumination with  $3.5 \text{ mW cm}^{-2}$  at 470 nm. The red dashed curves depict exponent (a) and double exponent (b) decay of the  $I_{\text{ph}}$ .

**Table 1.** Comparison of the main parameters of photodetectors based on individual SWCNT.

SWCNT modification	$V_{\text{DS}}$ [V]	$V_{\text{G}}$ [V]	Light intensity [ $\text{W cm}^{-2}$ ]	Wavelength [nm]	Responsivity [ $\text{A W}^{-1}$ ]
<i>p-n</i> junction in suspended SWCNT <sup>[12]</sup>	0.025	$\pm 2$	$< 10^3$	300-800	$0.2 \times 10^{-6}$
<i>p-n</i> junction in suspended sc-SWCNT in vacuum <sup>[8]</sup>	0	$\pm 8$	$1.45 \times 10^3$	532	$\sim 7 \times 10^{-6}$
SWCNT covered by $\text{MoS}_2$ <sup>[53]</sup>	0.1	0	$0.2 \times 10^{-3}$	532	300 <sup>a)</sup>
SWCNT/Si junction <sup>[4]</sup>	0	0	$< 13 \times 10^3$	825-1400	$0.5 \times 10^{-6}$
sc-SWCNT with asymmetric contact <sup>[54]</sup>	0	-3	-	830	$\sim 2 \times 10^{-9}$
sc-SWCNT covered by chromophore <sup>[55]</sup>	0.01	0	$10^{-2}$	400-600	$\sim 0.2$
SWCNT covered by photosensitive molecules <sup>[56]</sup>	0.2	-5	$6.25 \times 10^{-7}$	633	$7.7 \times 10^{5 \text{ a)}}$
sc-SWCNT covered by copolymer <sup>[48]</sup>	0.5	-6	$\sim 2$	400-700	$4 \times 10^{-6}$
<i>p-n</i> junction in s-SWCNT doped by oligomer <sup>[13]</sup>	0	0	7.1	1550	$180 \times 10^{-3}$
TPO-SWCNT/qm-SWCNT junction ( <i>this work</i> )	1	0	$5 \times 10^{-6}$	470-630	$51 \times 10^{-3}$ $2 \times 10^7$ <sup>a)</sup>

<sup>a)</sup> Recalculated responsivity for the active area of the device

A low-cost, facile, and versatile direct patterning technique based on femtosecond laser processing is reported. This method is applied to individual single-walled carbon nanotube transistors to convert quasi-metallic to semiconducting nanotubes by grafting oxygen species and form a planar junction between pristine and modified parts of a nanotube to detect ultralow light intensities in a broadband light range.

Aleksei V. Emelianov,\* Nikita P. Nekrasov, Maksim V. Moskotin, Georgy E. Fedorov, Nerea Otero, Pablo M. Romero, Vladimir K. Nevolin, Boris I. Afinogenov, Albert G. Nasibulin, and Ivan I. Bobrinetskiy

### Individual SWCNT Transistor with Photosensitive Planar Junction Induced by Two-Photon Oxidation

